Journal of Magnetic Resonance 352 (2023) 107460

Contents lists available at ScienceDirect

Journal of Magnetic Resonance

journal homepage: www.elsevier.com/locate/jmr

Enhanced sensitivity for pulse dipolar EPR spectroscopy using variable-time RIDME

Joshua L. Wort, Katrin Ackermann, Angeliki Giannoulis, Bela E. Bode

EaStCHEM School of Chemistry, Biomedical Sciences Research Complex and Centre of Magnetic Resonance, University of St Andrews, North Haugh, St Andrews, Scotland

ARTICLE INFO

Article history:
Received 14 January 2023
Revised 3 April 2023
Accepted 19 April 2023
Available online 25 April 2023

Keywords:
Distance measurements
Sensitivity
Double histidine
Spin-label

ABSTRACT

Pulse dipolar EPR spectroscopy (PDS) measurements are an important complementary tool in structural biology and are increasingly applied to macromolecular assemblies implicated in human health and disease at physiological concentrations. This requires ever higher sensitivity, and recent advances have driven PDS measurements into the mid-nanomolar concentration regime, though optimization and acquisition of such measurements remains experimentally demanding and time expensive. One important consideration is that constant-time acquisition represents a hard limit for measurement sensitivity, depending on the maximum measured distance. Determining this distance *a priori* has been facilitated by machine-learning structure prediction (AlphaFold2 and RoseTTAFold) but is often confounded by non-representative behaviour in frozen solution that may mandate multiple rounds of optimization and acquisition. Herein, we endeavour to simultaneously enhance sensitivity and streamline PDS measurement optimization to one-step by benchmarking a variable-time acquisition RIDME experiment applied to Cu^{II}-nitroxide and Cu^{II}-Cu^{II} model systems. Results demonstrate marked sensitivity improvements of both 5- and 6-pulse variable-time RIDME of between 2- and 5-fold over the constant-time analogues.

1. Introduction

Pulse dipolar electron paramagnetic resonance spectroscopy (PDS) has emerged as a powerful tool for characterisation of complex macromolecular assemblies, complementing atomic resolution of X-ray crystallography (XRC) [1,2] and cryo-electron microscopy (cryo-EM) [3,4], with distance constraints in the range of 1.5–16 nm [5–8]. Furthermore, PDS measurements are often performed in frozen solution on a molecular ensemble, ameliorating problems associated with sample crystallisation and immobilisation, as well as size limitations, and potential structural perturbations upon introduction of sterically bulky fluorophores, associated with XRC, cryo-EM, nuclear magnetic resonance (NMR) and Förster Resonance Energy Transfer (FRET), respectively. In this purview, PDS has provided insight into structural models [4,9–11], conformational [12–19] and binding equilibria [20–27], multimerization state [28–30], spin-counting [31–33], and kinetic landscapes [34–36]. For a comprehensive overview of the contributions of PDS to structural biology, the reader is directed to several excellent reviews [37–39]. Additionally, PDS is performed with continuously improving sensitivity, facilitating measurements down to concentrations of hundreds [40,41] and even tens of nM [23,42,43]. The motivation for enhanced measurement sensitivity is multi-faceted, but importantly allows for the study of protein and nucleic acid systems under near physiological concentrations and *in cellulo* [7,44–50].

Commercial instruments have been used successfully for pulse electron–electron double resonance (PELDOR) [51,52] (also known as double electron–electron resonance or DEER [53]) measurements at low μM concentration [54]. Concentration sensitivity can be further improved *via* homebuilt high-power resonator-free spectrometers [55,56], or by implementation of arbitrary waveform generators (AWGs) and shaped pulses that yield higher spin inversion efficiencies [57–62]. Furthermore, spin labels with exquisitely narrow spectral linewidths such as trityl radicals [43,63,64], have exceptional sensitivity when coupled with the single-frequency double quantum coherence (DQC) filtered [65] experiment. Yet another strategy for enhanced sensitivity involves the use of novel pulse sequences, either to prolong the transverse coherence of electron spins by reducing the influence of nuclear spin diffusion [66,67], improve the inversion efficiency of the microwave pulses and associated modulation depths [68,69], or through development and implementation of custom detection schemes [70,71].

While novel pulse sequences have achieved broad success at improving measurement sensitivity, constant-time acquisition

E-mail address: beb2@st-andrews.ac.uk (B.E. Bode)

https://doi.org/10.1016/j.jmr.2023.107460
1090-7807/

schemes are non-ideal from a sensitivity perspective. Briefly, constant-time acquisition has a total period of dipolar evolution (t_{max}) which is identical (i.e., constant) for all time-points throughout the measurement. This limits the achievable sensitivity in dependence of the t_{max}, and simultaneously mandates selection of t_{max} *a priori*, optimized for a particular inter-spin distance. Historically, this would require medium- to high-resolution structural data, but the advent of machine learning structural prediction tools (e.g., AlphaFold2 [72,73] and RoseTTAFold [74]) shows promise to overcome this bottle-neck. Importantly, constant-time acquisition normalizes the transverse dephasing experienced by the spin-labelled molecular ensemble, and therefore the relaxational contribution (including instantaneous diffusion under detection pulses) to the detected echo is fixed (i.e., sub-ensembles, regardless of differential transverse relaxation behaviour, will have identical contributions to the detected echo at each time-point throughout the measurement).

An alternative, so called 'variable-time acquisition', has a dynamic t_{max} which is incremented with each time-point throughout the measurement. This manifests as a sensitivity enhancement at short dipolar evolution times (i.e., at earlier time-points), which diminishes as the dipolar evolution time increases (i.e., at later time-points). This effectively decouples achievable sensitivity from t_{max}, which can be selected arbitrarily, and truncated in post-processing, facilitating one-step measurement optimization of systems with multimodal distance distributions (i.e., in cases where determination of an optimum t_{max} is problematic). Indeed, the variable-time 4-pulse DEER pulse sequence [75] demonstrated significant sensitivity enhancement compared to the constant-time analogue in rod-shaped persistent biradicals and in a transmembrane protein. However, sensitivity to sub-ensembles poses the problem of differential transverse dephasing [76,77] (e.g., *via* instantaneous diffusion) leading to different contributions arising at different t_{max} values. Subsequently, this cannot be processed with the standard Kernel assuming all time-points encode the same distance (and frequency) distribution, which has hindered widespread adoption and application. Despite this, attempts to hybridize the improved sensitivity of variable-time acquisition with the fixed relaxational contributions of constant-time acquisition format, have found some success [78,79].

Herein, we revisit variable-time acquisition in the context of the relaxation induced dipolar modulation enhancement (RIDME) [80–82] pulse sequence (shown for the 5- and 6-pulse experiments in Fig. 1a), and in light of several advances with respect to electron-nuclear modulation suppression [83] and nanomolar concentration sensitivity [20,23,40]. Interestingly, the original 3-pulse RIDME experiment benchmarked by Kulik *et al.* [81] used variable-time acquisition but was not dead-time free. In the variable-time dead-time free RIDME sequences used in this work, the position of the mixing block and the final refocusing pulse are all incremented at the same time (Fig. 1b). Relaxational contributions to the detected echo, and electron spin echo envelope modulation (ESEEM) are suppressed by deconvolution using a reference trace (i.e., where only the position of the final refocusing pulse is incremented in time, Fig. 1c, analogously to variable-time dead-time free DEER) yielding a trace containing only electron-nuclear modulations, (i.e., free of oscillations arising from dipolar coupling), and a stretched-exponential background decay, as an approximation of the product of an exponential and Gaussian decay term [84]. This is in contrast to the constant-time experiment wherein the position of the final refocusing pulse is decremented relative to the mixing block as the latter is incremented in time.

A series of 5- and 6-pulse variable-time dead-time free RIDME Cu^{II}-Cu^{II} and Cu^{II}-nitroxide measurements are benchmarked on a pair of *Streptococcus sp.* group G protein G, B1 domain (GB1) constructs, [20,85] and a nitroxide-labelled terpyridine ruler complexed with Cu^{II} [86] (Fig. 2) respectively. The performance of variable-time RIDME with respect to sensitivity and distance distribution reliability compared to the constant-time analogue is assessed. Additionally, the influence of deconvolution on sensitivity and distance distribution fidelity, as well as application of an extended phase-cycle [87] to suppress artefacts at short mixing times, particularly in the Cu^{II}-nitroxide 5-pulse variable-time RIDME measurements, are discussed and evaluated.

2. Experimental procedures

All protein expression, purification, labelling, and sample preparation (unless otherwise stated) were performed as previously described [20,88,89]. All data analysis was performed in DeerAnalysis2018, [90] raw data was fitted with a stretched exponential background function with dimension 3–6 (unless otherwise stated) and validations were performed as previously described [20,91]. Briefly, a 6-dimensional stretched exponential background function is assumed, and an initial validation (56 trials) is performed, consisting of 8 iterations of background start position (between 5 and 30% of the total RIDME trace length), and 7 iterations of background dimension (between 3 and 6 in increments of 0.5). Once the optimal background start position and background dimension are determined, the data are reloaded, processed using these values and a second validation (896 trials) is performed, consisting of the previous validation step and an additional 16 iterations of white noise (noise level 1.5).

Variable-time RIDME traces were deconvoluted (unless otherwise stated) by division with the experimental reference trace (see SI section 1.4 for details). Sensitivity per echo was calculated as previously described [92]. For further details on sample preparation, measurement parameters, and data analysis see SI sections 1.1, 1.3, and 1.4, respectively. The Bruker PulseSPEL programs corresponding to the variable-time 5- and 6-pulse RIDME experiments used in this work are given in the underpinning data [93]. The influence of the deconvolution procedure upon raw variable-time RIDME data is shown overleaf (Fig. 3). While we abstain from deconvoluting raw data with analytical stretched exponential functions fitted to the reference trace, it should be recognised that division in this way can mitigate noise explosion arising from division at long dipolar evolution times, (i.e., where signal intensity approaches 0) [94]. For the corresponding stretched exponential fits of all variable-time RIDME reference traces and residuals, see SI section 2.7.

3. Results and discussion

Firstly, 5- and 6-pulse constant- and variable-time Cu^{II}-Cu^{II} RIDME was applied to 100 μM I6H/N8H/K28H/Q32H GB1 in presence of 170 μM Cu^{II}-nitrilotriacetic acid (NTA) (Fig. 4); this protein to Cu^{II} ratio was previously shown to yield labelling corresponding to the sensitivity optimum [89] with a mixing time corresponding to 0.7 $\times T_1$. The results demonstrate that the variable-time measurements (blue and cyan traces, respectively) recapitulate the expected distance distributions, with a unimodal peak at $\sim$ 2.5 nm, consistent with both the 5- and 6-pulse constant-time RIDME measurements (red and green traces, respectively). We also calculated the root mean square deviation (RMSD) of the corresponding distance distribution error estimates and found all values to be comparable: the 5- and 6-pulse constant-time RIDME measurements had RMSD values of 5.40×10^{-2} and 6.28×10^{-2}, respectively. The 5- and 6-pulse variable-time RIDME measurements had RMSD values of 6.93×10^{-2} and 5.96×10^{-2}, respectively. It is observed that prior to deconvolution the variable-time RIDME measurements consistently have a steeper background decay com-

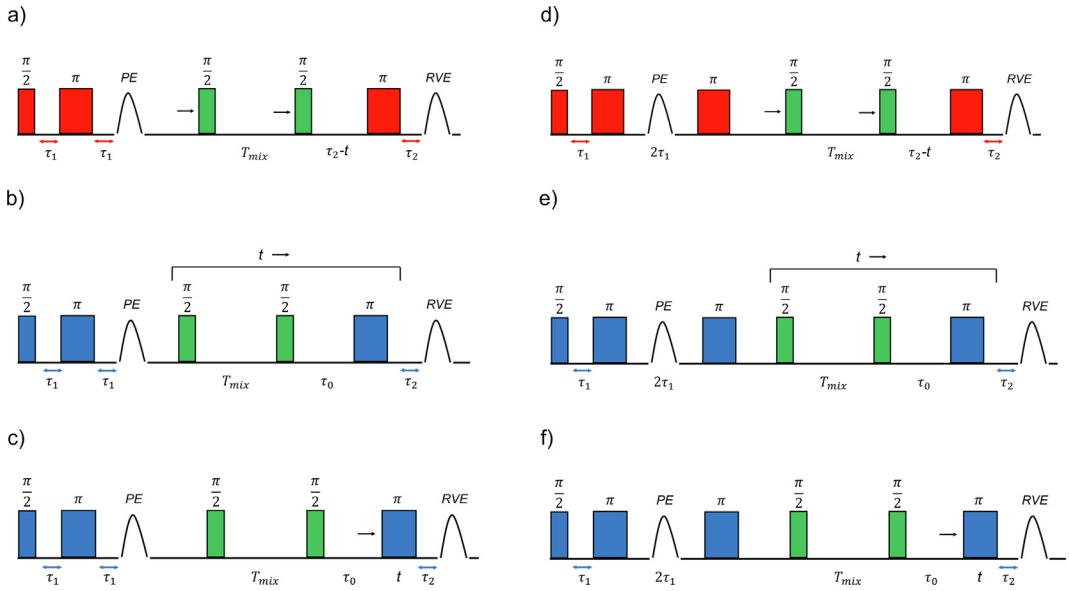

Fig. 1. a) 5-pulse constant-time ridme pulse sequence, with detection pulses indicated in red, and mixing block interval (T_{mix}) pulses indicated in green. The position of the mixing block is incremented in time by t, indicated by the black arrows. The interval between detection pulses in the Hahn echo subsequence (τ_1) and the total dipolar evolution time (τ_2) are indicated by the double-headed red arrows. The position of the final π-pulse is constant, separated by $\tau_2 - t$ from the mixing block. b) 5-pulse variable-time RIDME pulse sequence, with detection pulses indicated in blue, and mixing block interval pulses in green. The intervals τ_1 and τ_2 are indicated by the double-headed blue arrows. Here, the position of the mixing block and the final π-pulse are incremented together in time by t (i.e., the position of the final π-pulse is dynamic, separated by an arbitrarily short time interval (τ_0) from the mixing block. c) 5-pulse variable-time RIDME reference pulse sequence, with detection pulses indicated in blue, and mixing block interval pulses in green. The intervals τ_1 and τ_2 are indicated as in b). Here, only the position of final π-pulse is incremented in time by t, to isolate relaxational contributions to the detected echo without dipolar contributions arising from incrementing the mixing block. PE and RVE refer to primary echo and refocussed virtual echo, respectively. d) 6-pulse constant-time RIDME pulse sequence with colour scheme and labelling as in a). e) 6-pulse variable-time RIDME experimental pulse sequence with colour scheme and labelling as in b). f) 6-pulse variable-time RIDME reference pulse sequence with colour scheme and labelling as in c). (For interpretation of the references to colour in this figure legend, the reader is referred to the web version of this article.)

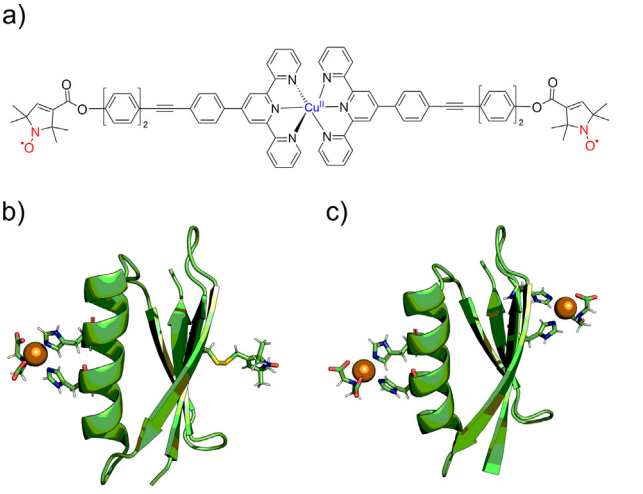

Fig. 2. a) Terpyridine-based synthetic model system containing nitroxide moieties and complexed by Cu^{II}. b) and c) I6R1/K28H/Q32H and I6H/N8H/K28H/Q32H GB1 constructs, respectively, shown in cartoon representation. The R1 sidechain, double-histidine motifs, and NTA ligands are shown in stick representation. The Cu^{II} spin centres are shown as brown spheres.

pared to the constant-time RIDME measurements, with the division leading to a decrease in the steepness of the background decay (see SI section 2.3 for discussion). The observation of a slower background decay for variable-time RIDME after deconvolution is rationalized by the removal of electron-nuclear (ESEEM) modulations and dipolar modulations that already manifested at short mixing times, which in the non-deconvoluted trace represent additional pathways for dephasing accelerating background decay. Furthermore, this increased steepness was borne-out by simulation of background decay shape assuming a dynamic t_{max} parameter, (i.e., the unmodulated component of the detected echo is not a constant attenuating factor), and product of stretched exponentials (see SI section 2.1 for discussion).

While the distance distributions were highly robust and consistent regardless of the RIDME pulse sequence used, it should be noted that for distance distributions that are broad, or contain long distances such that dipolar oscillations are not well pronounced, then imperfections in the deconvolution may affect the determined distance distribution. Additionally, we compared their relative sensitivities, to determine potential gains *via* the variable-time acquisition scheme. The 5- and 6-pulse constant-time RIDME measurements had sensitivities per echo of 8.43×10^{-1} and 4.85×10^{-1}, respectively. This is consistent with a recent systematic comparison that observed reduced sensitivity in 6-pulse RIDME [95], due to imperfect refocussing by the additional π-pulse in the Carr-Purcell subsequence. Significantly, the 5- and 6-pulse variable-time RIDME measurements had sensitivities per echo of 1.47 and 1.27, representing modest improvements in sensitivity over the constant-time analogous measurements by factors > 1.7 and > 2.5, respectively. Interestingly, the sensitivities per echo do not directly reflect a lower RMSD in the distance distribution error bounds. We propose this arises because the ground truth error bounds for the distance distributions are not available and so are only approximated by the Tikhonov validations. An increased distance distribution RMSD may additionally manifest from uncertainties in variable-time RIDME deconvolution and background removal.

Furthermore, omission of the deconvolution step of variable-time RIDME traces in pre-processing, nominally used to suppress ESEEM and relaxational contributions to the modulated signal, yielded a further sensitivity enhancement (see SI section 2.3 for

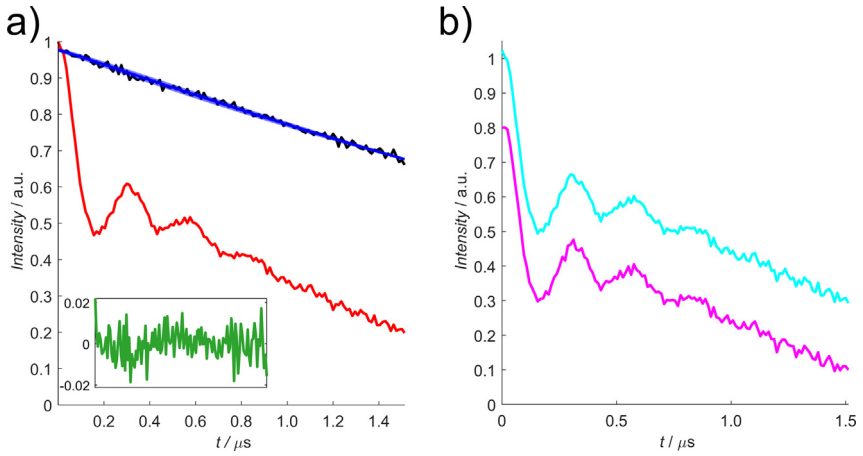

Fig. 3. a) 5-pulse variable-time RIDME reference trace (pulse sequence shown in Fig. 1 c) (black trace) fitted with a stretched exponential function (blue trace) with the 95% confidence bounds indicated by the shaded regions (barely visible), and raw variable-time RIDME data prior to deconvolution (pulse sequence shown in Fig. 1 b) (red trace). Inset: A plot of residuals of the fitted stretched exponential function to the variable-time RIDME reference trace, green trace. b) 5-pulse variable-time RIDME data deconvoluted with i) the analytical stretched exponential function (cyan trace), and ii) the experimental reference trace (magenta trace, shifted by −0.2 vertically). (For interpretation of the references to colour in this figure legend, the reader is referred to the web version of this article.)

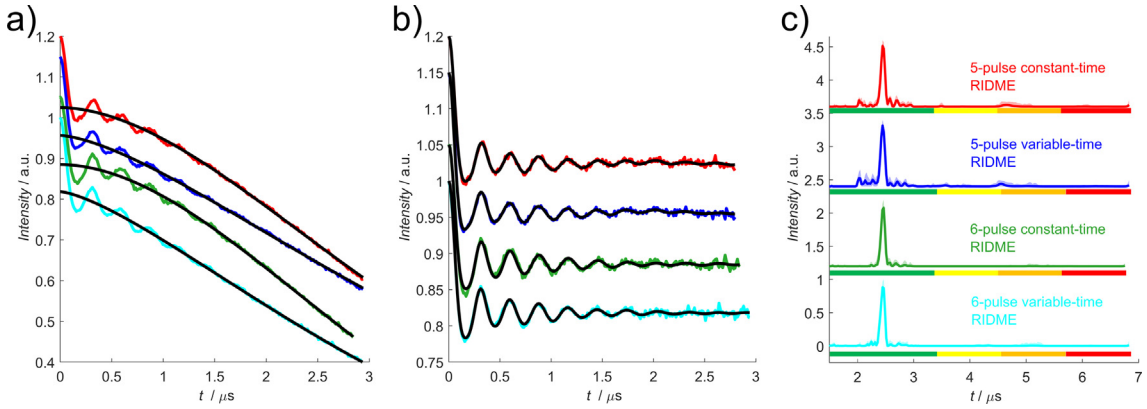

Fig. 4. 5- (red) and 6- (green) pulse constant-time, and 5- (blue) and 6- (cyan) pulse deconvoluted Cu^{II}-Cu^{II} variable-time RIDME measurements of 100 μM I6H/N8H/K28H/Q32H GB1 in presence of 170 μM Cu^{II}-NTA. a) primary data with black traces corresponding to the fitted stretched exponential background functions, b) dipolar evolution functions with black traces corresponding to the Tikhonov fits from DeerAnalysis and c) corresponding validated distance distributions. In c) the 95% confidence estimates ($\pm$ 2 σ) are shown as shaded regions and the colour bar indicates reliability ranges (green: shape reliable; yellow: mean and width reliable; amber: mean reliable; red: no quantification possible). (For interpretation of the references to colour in this figure legend, the reader is referred to the web version of this article.)

discussion). Surprisingly, the distance distributions reconciled nicely with constant-time RIDME data, even when variable-time RIDME data was not deconvoluted. Here, 5- and 6-pulse variable-time RIDME measurements had sensitivities per echo of 2.66, and 2.37, representing improved sensitivity over constant-time measurements by factors $>$ 3.0 and $>$ 4.8, respectively. However, ignoring the relaxational contributions to the detected echo is likely only feasible when considering short distances, and where differential relaxation behaviour of sub-ensembles is negligible, both yet to be evaluated experimentally.

Next, 5- and 6-pulse constant- and variable-time Cu^{II}-nitroxide RIDME was applied to 100 μM nitroxide-labelled terpyridine ligand in presence of 50 μM Cu^{II} (Fig. 5). All measurements recapitulate the expected distance distribution, with comparable RMSD, the 5- and 6-pulse variable-time RIDME measurements had RMSD values of 2.92 $\times$ 10^{-1} and 1.10 $\times$ 10^{-1}, respectively. The 5-pulse constant-time RIDME measurement had RMSD value of 1.98 $\times$ 10^{-1}, however it should be noted that the 6-pulse constant-time RIDME measurement is background corrected with a fourth-order polynomial (i.e., the distance distribution does not contain error bounds). This empirical background correction has been used for 6-pulse RIDME previously [82] and using a stretched exponential background function resulted in a dimension of < 3. Additionally, it was observed that Cu^{II}-nitroxide 5-pulse variable-time RIDME reference measurements did not contain the low-frequency artefact, meaning that deconvolution led to amplification of the artefact in experimental traces (see SI section 2.2 for discussion). Furthermore, recording 5-pulse variable-time RIDME measurements with a short mixing time (T_{ref}) introduced additional artefacts (i.e., potentially from crossing of echoes with coherence order $\neq$0 during the mixing block). Therefore, an extended 32-step phase-cycle [87] was applied (see SI section 2.2 for discussion) and sufficiently suppressed artefacts to allow deconvolution by measurements with a short mixing time (akin to previous 5-pulse constant-time RIDME measurements [21,22,24]). The mismatch between the simulation and experiment in the first minimum of the time domain data is attributed to effects arising from the rigidity of the model system paired with orientation selection in the RIDME experiment [96].

The 5- and 6-pulse constant-time RIDME measurements had sensitivities per echo of 1.11 $\times$ 10^{1} and 1.15, respectively. Importantly, such large sensitivity difference (approximately an order

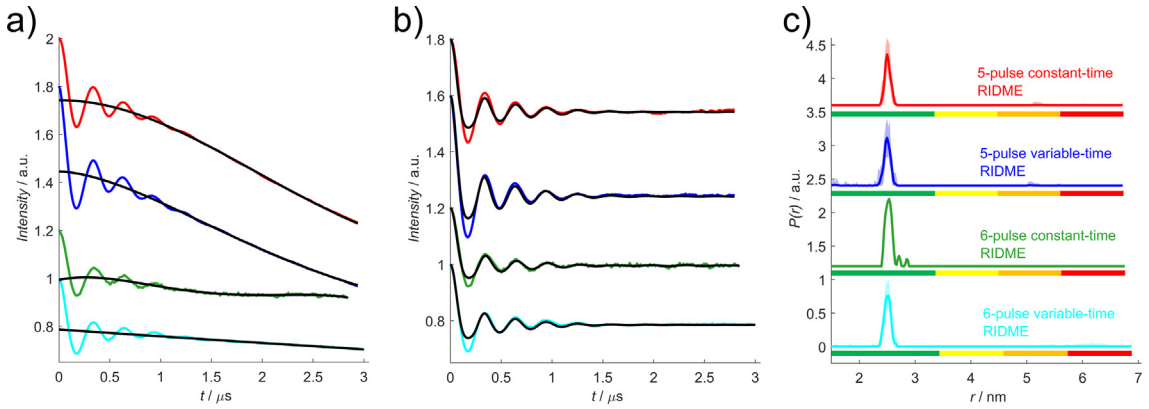

Fig. 5. 5- (red) and 6- (green) pulse constant-time, and 5- (blue) and 6- (cyan) pulse deconvoluted Cu^{II}-nitroxide variable-time RIDME measurements of 100 μM nitroxide-labelled terpyridine ligand in presence of 50 μM Cu^{II}. Note that the 5-pulse constant-time RIDME data is deconvoluted, while the analogous 6-pulse RIDME data is not. Additionally, 6-pulse constant-time RIDME is background corrected assuming a fourth-order polynomial. a)-c) as in Fig. 4. (For interpretation of the references to colour in this figure legend, the reader is referred to the web version of this article.)

of magnitude) is likely to be non-representative and arises from i) overfitting of the low-frequency artefact in the 5-pulse constant-time RIDME which inflates the estimated modulation depth (i.e., the amplitude between the signal intensity at time zero and the time when the signal is entirely damped in the limit of negligible intermolecular decay), and ii) RMSD determined from the imaginary component of the RIDME trace being dominated by dipolar oscillations rather than thermal noise. Comparatively, the 5- and 6-pulse variable-time RIDME measurements had sensitivities per echo of 1.19×10^{1} and 4.16, respectively, representing only marginal sensitivity improvement for the 5-pulse RIDME experiment, and a factor > 3.6 for the 6-pulse RIDME experiment.

However, in cases with high signal-to-noise ratio (SNR), quantification of RMSD, and subsequently sensitivity becomes less robust (*vide supra* point ii). Interestingly, Cu^{II}-nitroxide 5- and 6-pulse RIDME measurements performed at X-band frequency (analogous to data shown in Fig. 4) demonstrated a sensitivity enhancement for variable-time acquisition of ∼ 2.0, compared to constant-time acquisition (see SI section 2.4 for details). Therefore, to investigate more robustly the sensitivity advantage of 5-pulse variable-time over constant-time RIDME, low concentration Cu^{II}-Cu^{II} (5 μM I6H/N8H/K28H/Q32H GB1 in presence of 10 μM Cu^{II}-NTA) and Cu^{II}-nitroxide (0.5 μM I6R1/K28H/Q32H GB1 in presence of 2.7 μM Cu^{II}-NTA) RIDME samples were prepared and measured (Fig. 6). At these limiting concentrations, sensitivity enhancements afforded by variable-time acquisition should become more apparent and easier to quantify, as estimation of RMSD from the imaginary component is more reliable.

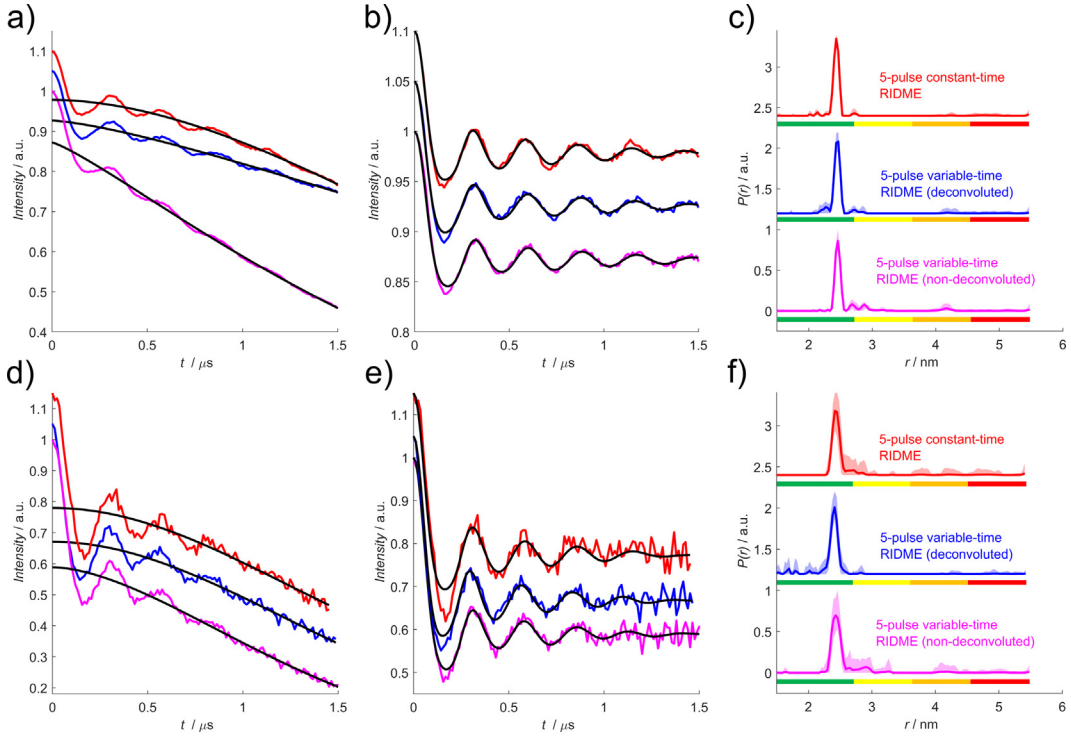

Fig. 6. Top) 5-pulse constant-time (red), variable-time deconvoluted (blue), and variable-time non-deconvoluted (magenta) Cu^{II}-Cu^{II} RIDME measurements of 5 μM I6H/N8H/K28H/Q32H GB1 in presence of 10 μM Cu^{II}-NTA. Bottom) 5-pulse constant- and variable-time Cu^{II}-nitroxide RIDME measurements of 0.5 μM I6R1/K28H/Q32H GB1 in presence of 2.7 μM Cu^{II}-NTA, with the same colour scheme as above. a)-c) and d)-f) as in Fig. 3. (For interpretation of the references to colour in this figure legend, the reader is referred to the web version of this article.)

Constant-time RIDME traces are non-deconvoluted (red traces) and variable-time RIDME traces are either deconvoluted with a reference trace (blue traces) or non-deconvoluted (magenta traces).

The Cu^{II}-Cu^{II} constant-time, deconvoluted variable-time and non-deconvoluted variable-time RIDME measurements had sensitivities per echo of 5.44×10^{-2}, 9.90×10^{-2}, and 1.00×10^{-1}, respectively. This represents a sensitivity enhancement by a factor > 1.8 for non-deconvoluted variable-time RIDME with respect to constant-time RIDME, highly consistent with the factor > 1.7 observed for the initial 5-pulse variable-time Cu^{II}-Cu^{II} RIDME measurements (Fig. 4). Concomitantly, the Cu^{II}-nitroxide constant-time, deconvoluted variable-time and non-deconvoluted variable-time RIDME measurements had sensitivities per echo of 3.52×10^{-1}, 5.29×10^{-1}, and 7.37×10^{-1}, respectively. This represents a sensitivity enhancement by a factor ~ 2.1 for non-deconvoluted variable-time RIDME with respect to the constant-time analogue, which is markedly higher than the enhancement observed in the nitroxide-labelled terpyridine variable-time RIDME measurements (Fig. 5).

Once again, the distance distributions are highly consistent between constant- and variable-time RIDME measurements independent of whether deconvolution with a reference trace during pre-processing is performed. Here, the RMSD values for the distance distribution error bounds for the Cu^{II}-nitroxide measurements were 3.32×10^{-1}, 3.06×10^{-1}, and 2.80×10^{-1} for constant-time, variable-time, and variable-time deconvoluted, respectively. Correspondingly, for the Cu^{II}-Cu^{II} measurements RMSD values were 3.19×10^{-2}, 4.33×10^{-2}, and 4.51×10^{-2}, for constant-time, variable-time, and variable-time deconvoluted, respectively.

However, the results also indicate there is clearly a trade-off between the background decay steepness and sensitivity enhancement (i.e., omission of the deconvolution step increases sensitivity nominally by a factor of 2 (the product of a factor $\sqrt{2}$ in acquisition time, and a factor $\sqrt{2}$ owing to the deconvolution itself) but leads to considerably steeper background decay, especially in the Cu^{II}-Cu^{II} case). Since the RIDME background decay is primarily dominated by electron-nuclear spectral diffusion during the mixing block interval, measuring at higher temperatures (i.e., with faster longitudinal relaxation behaviour and subsequently shorter mixing times) can ameliorate prohibitive background decays. Indeed, a systematic sensitivity analysis of Cu^{II}-Cu^{II} variable-time RIDME measurements performed at different temperatures and mixing times indicated a global optimum at 40 K and a mixing time equivalent to the longitudinal relaxation time constant, T_1 of 15 μs (see SI section 2.6 for discussion).

4. Conclusions

In summary, we have established a variable-time acquisition scheme of the 5- and 6-pulse RIDME experiments, benchmarked on Cu^{II}-Cu^{II} and Cu^{II}-nitroxide systems. Taken together, results demonstrate that variable-time acquisition affords approximately a factor 2 sensitivity enhancement compared to the constant-time analogue, even at sub-μM concentrations. Significantly, this marks a factor 4 reduction in the acquisition time, where the limit is approximately ~ 60 h with existing hardware in our hands (i.e., phase drifts become significant at this time scale) [23,40]. Combination of variable-time RIDME measurements with trityl radicals as the detected spin, use of cryogenically cooled pre-amplifiers [97], and non-uniform sampling [98], may offer further sensitivity enhancements even down to single digit nM concentrations, extending the scope of PDS distance measurements towards systems predisposed to precipitate above a limiting concentration threshold, or where material is otherwise limited (i.e., poor purification yield, or lack of available heterologous expression [99]).

Perhaps more importantly, results also indicate that in certain cases (i.e., conditional on the caveat of short distances where differences in relaxation behaviour between sub-ensembles is assumed to be negligible) variable-time RIDME deconvolution is sometimes unnecessary to accurately recapitulate distance distributions when compared with the constant-time RIDME experiment. While this is likely to be strongly system-dependent, it suggests that variable-time RIDME is especially well-suited to measure short inter-spin distances (1.5–3.0 nm) with improved sensitivity. Improved SNR at the early time-points (i.e., before the dipolar oscillation is damped) may also make variable-time RIDME valuable for measurement of mid- (3.5–6.0 nm) and long-range distances ($\geq$6.0 nm), even in cases where the background decay is prohibitively steep and reduces the achievable t_{max}.

The measured distances in this work are short ($\sim$2.5 nm), and therefore one open question is how robustly variable-time RIDME provides reliable distance distributions when applied to systems containing longer or broader distances. Interestingly, the sensitivity enhancement afforded by variable-time compared to constant-time RIDME may facilitate measurement at higher temperatures (optimally in a range where T_m is largely constant) where background decay is shallower and subsequently extends the achievable t_{max} above the noise floor. Furthermore, it should be cautioned that for longer distances (i.e., where the dipolar oscillation period is comparable to or exceeds the T_m) variable-time RIDME traces may have lower SNR due to a steeper decay and owing to the deconvolution causing a noise explosion at the end of the trace.

Finally, it is hoped that variable-time RIDME opens avenues toward more efficient measurement optimisation, being robust to deviations between *in silico* and solution-state structures, that would otherwise mandate repetition of measurements with different dipolar evolution times before the optimum t_{max} is found. In fact, because a variable-time RIDME trace is essentially composed of several constant-time RIDME traces with different t_{max} values, incremental truncation and global fitting [100] may improve accuracy and robustness of distance distribution determination. Furthermore, with the recent drive towards streamlining of PDS workflows (i.e., automation of data analysis [101–103], parameter and measurement optimisation [104], and structural interpretation of PDS distance constraints [105]), shifting to variable-time acquisition offers to simplify experimental set-up and ameliorate issues associated with subjective data truncation during post-processing.

The research data supporting this publication can be accessed at https://doi.org/10.17630/db46fa7d-13c5-49ef-aa07-847ab67c7bca [93].

CRediT authorship contribution statement

Joshua L. Wort: Conceptualization, Investigation, Data curation, Formal analysis, Methodology, Writing – original draft, Writing – review & editing. **Katrin Ackermann:** Investigation, Writing – review & editing. **Angeliki Giannoulis:** Investigation, Writing – review & editing. **Bela E. Bode:** Conceptualization, Investigation, Formal analysis, Funding acquisition, Methodology, Supervision, Writing – review & editing.

Data availability

Data will be deposited in institutional repository upon publication.

Declaration of Competing Interest

The authors declare that they have no known competing financial interests or personal relationships that could have appeared to influence the work reported in this paper.

Acknowledgement

For the purpose of open access, the authors have applied a Creative Commons Attribution (CC BY) licence to any Accepted Author Manuscript version arising. We thank the StAnD (St Andrews and Dundee) EPR group for long-standing support and in particular Dr El Mkami for assistance with PDS experiments. J. L. W. acknowledges support by the BBSRC DTP Eastbio (BB/M010996/1). A. G. acknowledges the EPSRC-funded Centre for Doctoral Training in 'integrated magnetic resonance', iMR-CDT (EP/J500045/1) B. E. B. and K. A. acknowledge support by the Leverhulme Trust (RPG-2018-397) and EPSRC (EP/X016455/1). B. E. B. acknowledges equipment funding by BBSRC (BB/R013780/1 and BB/T017740/1).

Appendix A. Supplementary material

Supplementary data to this article can be found online at https://doi.org/10.1016/j.jmr.2023.107460.

References

[1] J.E. Besaw, J. Reichenwallner, P. De Guzman, A. Tucs, A. Kuo, T. Morizumi, K. Tsuda, A. Sljoka, R.J.D. Miller, O.P. Ernst, Sci. Rep. 12 (2022) 13955.
[2] N. Alonso-García, I. García-Rubio, J.A. Manso, R.M. Buey, H. Urien, A. Sonnenberg, G. Jeschke, J.M. de Pereda, Acta Crystallogr. Sect. D Biol. Crystallogr. 71 (2015) 969–985.
[3] D.Y. Zhao, M. Pöge, T. Morizumi, S. Gulati, N. Van Eps, J. Zhang, P. Miszta, S. Filipek, J. Mahamid, J.M. Plitzko, W. Baumeister, O.P. Ernst, K. Palczewski, J. Biol. Chem. 294 (2019) 14215–14230.
[4] T.M. Thaker, S. Mishra, W. Zhou, M. Mohan, Q. Tang, J.D. Faraldo-Goméz, H.S. Mchaourab, T.M. Tomasiak, Nat. Chem. Biol. 18 (2022) 226–235.
[5] T. Schmidt, M.A. Wälti, J.L. Baber, E.J. Hustedt, G.M. Clore, Angew. Chemie Int. Ed. 55 (2016) 15905–15909.
[6] B. Endeward, Y. Hu, G. Bai, G. Liu, T.F. Prisner, X. Fang, Biophys. J. 121 (2022) 37–43.
[7] O. Schiemann, C.A. Heubach, D. Abdullin, K. Ackermann, M. Azarkh, E.G. Bagryanskaya, M. Drescher, B. Endeward, J.H. Freed, L. Galazzo, D. Goldfarb, T. Hett, L. Esteban Hofer, L. Fábregas Ibáñez, E.J. Hustedt, S. Kucher, I. Kuprov, J.E. Lovett, A. Meyer, S. Ruthstein, S. Saxena, S. Stoll, C.R. Timmel, M. Di Valentin, H.S. Mchaourab, T.F. Prisner, B.E. Bode, E. Bordignon, M. Bennati, G. Jeschke, J. Am. Chem. Soc. 143 (2021) 17875–17890.
[8] M. Seal, O. Weil-Ktorza, D. Despotović, D.S. Tawfik, Y. Levy, N. Metanis, L.M. Longo, D. Goldfarb, J. Am. Chem. Soc. 144 (2022) 14150–14160.
[9] J. Casto, A. Mandato, L. Hofmann, I. Yakobov, S. Ghosh, S. Ruthstein, S. Saxena, Chem. Sci. 13 (2022) 1693–1697.
[10] P.S. Kerry, H.L. Turkington, K. Ackermann, S.A. Jameison, B.E. Bode, J. Phys. Chem. B 118 (2014) 10882–10888.
[11] C. Rouillon, N. Schneberger, H. Chi, K. Blumenstock, S. Da Vela, K. Ackermann, J. Moecking, M.F. Peter, W. Boenigk, R. Seifert, B.E. Bode, J.L. Schmid-Burgk, D. Svergun, M. Geyer, M.F. White, G. Hagelueken, Nature (2022) 1–23.
[12] H. Sameach, S. Ghosh, L. Gevorkyan-Airapetov, S. Saxena, S. Ruthstein, Angew. Chemie Int. Ed. 58 (2019) 3053–3056.
[13] C. Kapsalis, B. Wang, H. El Mkami, S.J. Pitt, J.R. Schnell, T.K. Smith, J.D. Lippiat, B.E. Bode, C. Pliotas, Nat. Commun. 10 (2019) 4619.
[14] A.M. Stewart, M. Shanmugam, R.J. Kutta, N.S. Scrutton, J.E. Lovett, S. Hay, Biochemistry 61 (2022) 1735–1742.
[15] A. Gopinath, B. Joseph, Angew. Chemie Int. Ed. 61 (2022) e202113448.
[16] G. Walke, J. Aupič, H. Kashoua, P. Janoš, S. Meron, Y. Shenberger, Z. Qasem, L. Gevorkyan-Airapetov, A. Magistrato, S. Ruthstein, Biophys. J. 121 (2022) 1194–1204.
[17] N. Van Eps, L.N. Caro, T. Morizumi, A.K. Kusnetzow, M. Szczepek, K.P. Hofmann, T.H. Bayburt, S.G. Sligar, O.P. Ernst, W.L. Hubbell, Proc. Natl. Acad. Sci. 114 (2017) E3268–E3275.
[18] L. Galazzo, G. Meier, M.H. Timachi, C.A.J. Hutter, M.A. Seeger, E. Bordignon, Proc. Natl. Acad. Sci. 117 (2020) 2441–2448.
[19] O.A. Krumkacheva, G.Y. Shevelev, A.A. Lomzov, N.S. Dyrkheeva, A.A. Kuzhelev, V.V. Koval, V.M. Tormyshev, Y.F. Polienko, M.V. Fedin, D.V. Pyshnyi, O.I. Lavrik, E.G. Bagryanskaya, Nucleic Acids Res. 47 (2019) 7767–7780.
[20] J.L. Wort, K. Ackermann, A. Giannoulis, A.J. Stewart, D.G. Norman, B.E. Bode, Angew. Chemie Int. Ed. 58 (2019) 11681–11685.
[21] J.L. Wort, S. Arya, K. Ackermann, A.J. Stewart, B.E. Bode, J. Phys. Chem. Lett. 12 (2021) 2815–2819.
[22] M. Oranges, J.L. Wort, M. Fukushima, E. Fusco, K. Ackermann, B.E. Bode, J. Phys. Chem. Lett. 13 (2022) 7847–7852.
[23] K. Ackermann, J.L. Wort, B.E. Bode, Chem. Commun. 58 (2022) 8790–8793.
[24] A. Giannoulis, M. Oranges, B.E. Bode, ChemPhysChem 18 (2017) 2318–2321.
[25] E.R. Georgieva, P.P. Borbat, H.D. Norman, J.H. Freed, Sci. Rep. 5 (2015) 11757.
[26] N. Erlenbach, C. Grünewald, B. Krstic, A. Heckel, T.F. Prisner, RNA 25 (2019) 239–246.
[27] N. Kubatova, T. Schmidt, C.D. Schwieters, G.M. Clore, Proc. Natl. Acad. Sci. 2023 (2017) 120.
[28] S. Milikisiyants, S. Wang, R.A. Munro, M. Donohue, M.E. Ward, D. Bolton, L.S. Brown, T.I. Smirnova, V. Ladizhansky, A.I. Smirnov, J. Mol. Biol. 429 (2017) 1903–1920.
[29] T. Schmidt, R. Ghirlando, J. Baber, G.M. Clore, ChemPhysChem 17 (2016) 2987–2991.
[30] L.M. Stratmann, Y. Kutin, M. Kasanmascheff, G.H. Clever, Angew. Chemie Int. Ed. 60 (2021) 4939–4947.
[31] A.D. Milov, A.B. Ponomarev, Y.D. Tsvetkov, J. Struct. Chem. 25 (1985) 710–713.
[32] B.E. Bode, D. Margraf, J. Plackmeyer, G. Dürner, T.F. Prisner, O. Schiemann, J. Am. Chem. Soc. 129 (2007) 6736–6745.
[33] M. Bretschneider, P.E. Spindler, O.Y. Rogozhnikova, D.V. Trukhin, B. Endeward, A.A. Kuzhelev, E. Bagryanskaya, V.M. Tormyshev, T.F. Prisner, J. Phys. Chem. Lett. 11 (2020) 6286–6290.
[34] T. Hett, T. Zbik, S. Mukherjee, H. Matsuoka, W. Bönigk, D. Klose, C. Rouillon, N. Brenner, S. Peuker, R. Klement, H.-J. Steinhoff, H. Grubmüller, R. Seifert, O. Schiemann, U.B. Kaupp, J. Am. Chem. Soc. 143 (2021) 6981–6989.
[35] A. Collauto, H.A. DeBerg, R. Kaufmann, W.N. Zagotta, S. Stoll, D. Goldfarb, Phys. Chem. Chem. Phys. 19 (2017) 15324–15334.
[36] T. Schmidt, J. Jeon, W.-M. Yau, C.D. Schwieters, R. Tycko, G.M. Clore, Proc. Natl. Acad. Sci. 119 (2022).
[37] D. Goldfarb, J. Magn. Reson. 306 (2019) 102–108.
[38] G. Jeschke, Emerg. Top. Life Sci. 2 (2018) 9–18.
[39] O. Schiemann, T.F. Prisner, Q. Rev. Biophys. 40 (2007) 1–53.
[40] K. Ackermann, J.L. Wort, B.E. Bode, J. Phys. Chem. B 125 (2021) 5358–5364.
[41] S. Kucher, C. Elsner, M. Safonova, S. Maffini, E. Bordignon, J. Phys. Chem. Lett. 12 (2021) 3679–3684.
[42] N. Fleck, C.A. Heubach, T. Hett, F.R. Haege, P.P. Bawol, H. Baltruschat, O. Schiemann, Angew. Chemie Int. Ed. 59 (2020) 9767–9772.
[43] N. Fleck, C. Heubach, T. Hett, S. Spicher, S. Grimme, O. Schiemann, Chem. – A Eur. J. 27 (2021) 5292–5297.
[44] F.X. Theillet, A. Binolfi, B. Bekei, A. Martorana, H.M. Rose, M. Stuiver, S. Verzini, D. Lorenz, M. Van Rossum, D. Goldfarb, P. Selenko, Nature 530 (2016) 45–50.
[45] R. Igarashi, T. Sakai, H. Hara, T. Tenno, T. Tanaka, H. Tochio, M. Shirakawa, J. Am. Chem. Soc. 132 (2010) 8228–8229.
[46] M. Azarkh, A. Bieber, M. Qi, J.W.A. Fischer, M. Yulikov, A. Godt, M. Drescher, J. Phys. Chem. Lett. 10 (2019) 1477–1481.
[47] I. Krstić, R. Hänsel, O. Romainczyk, J.W. Engels, V. Dötsch, T.F. Prisner, Angew. Chemie Int. Ed. 50 (2011) 5070–5074.
[48] Y. Yang, S.-N. Chen, F. Yang, X.-Y. Li, A. Feintuch, X.-C. Su, D. Goldfarb, Proc. Natl. Acad. Sci. 117 (2020) 20566–20575.
[49] B. Joseph, A. Sikora, D.S. Cafiso, J. Am. Chem. Soc. 138 (2016) 1844–1847.
[50] Y. Shenberger, L. Gevorkyan-Airapetov, M. Hirsch, L. Hofmann, S. Ruthstein, bioRxiv Prepr. (2022), https://doi.org/10.1101/2022.08.03.502720.
[51] R.E. Martin, M. Pannier, F. Diederich, V. Gramlich, M. Hubrich, H.W. Spiess, Angew. Chemie Int. Ed. 37 (1998) 2833–2837.
[52] A.D. Milov, A.B. Ponomarev, Y.D. Tsvetkov, Chem. Phys. Lett. 110 (1984) 67–72.
[53] M. Pannier, S. Veit, A. Godt, G. Jeschke, H.W. Spiess, J. Magn. Reson. 142 (2000) 331–340.
[54] E.S. Babaylova, A.A. Malygin, A.A. Lomzov, D.V. Pyshnyi, M. Yulikov, G. Jeschke, O.A. Krumkacheva, M.V. Fedin, G.G. Karpova, E.G. Bagryanskaya, Nucleic Acids Res. 44 (2016) 7935–7943.
[55] P.A.S. Cruickshank, D.R. Bolton, D.A. Robertson, R.I. Hunter, R.J. Wylde, G.M. Smith, Rev. Sci. Instrum. 80 (2009).
[56] W. Hofbauer, K.A. Earle, C.R. Dunnam, J.K. Moscicki, J.H. Freed, Rev. Sci. Instrum. 75 (2004) 1194–1208.
[57] A. Doll, M. Qi, A. Godt, G. Jeschke, J. Magn. Reson. 273 (2016) 73–82.
[58] C.L. Motion, S.L. Cassidy, P.A.S. Cruickshank, R.I. Hunter, D.R. Bolton, H. El Mkami, S. Van Doorslaer, J.E. Lovett, G.M. Smith, J. Magn. Reson. 278 (2017) 122–133.
[59] P.E. Spindler, Y. Zhang, B. Endeward, N. Gershernzon, T.E. Skinner, S.J. Glaser, T.F. Prisner, J. Magn. Reson. 218 (2012) 49–58.
[60] A. Doll, S. Pribitzer, R. Tschaggelar, G. Jeschke, J. Magn. Reson. 230 (2013) 27–39.
[61] P.E. Spindler, S.J. Glaser, T.E. Skinner, T.F. Prisner, Angew. Chemie Int. Ed. 52 (2013) 3425–3429.
[62] F.D. Breitgoff, K. Keller, M. Qi, D. Klose, M. Yulikov, A. Godt, G. Jeschke, J. Magn. Reson. 308 (2019).
[63] G.W. Reginsson, N.C. Kunjir, S.T. Sigurdsson, O. Schiemann, Chem. - A Eur. J. 18 (2012) 13580–13584.
[64] Z. Yang, Y. Liu, P. Borbat, J.L. Zweier, J.H. Freed, W.L. Hubbell, J. Am. Chem. Soc. 134 (2012) 9950–9952.
[65] P.P. Borbat, J.H. Freed, Chem. Phys. Lett. 313 (1999) 145–154.

[66] P.P. Borbat, E.R. Georgieva, J.H. Freed, J. Phys. Chem. Lett. 4 (2013) 170–175.
[67] P.E. Spindler, I. Waclawska, B. Endeward, J. Plackmeyer, C. Ziegler, T.F. Prisner, J. Phys. Chem. Lett. 6 (2015) 4331–4335.
[68] T. Bahrenberg, Y. Yang, D. Goldfarb, A. Feintuch, Magnetochemistry 5 (2019) 20.
[69] A. Doll, M. Qi, S. Pribitzer, N. Wili, M. Yulikov, A. Godt, G. Jeschke, Phys. Chem. Chem. Phys. 17 (2015) 7334–7344.
[70] S. Milikisiyants, M.A. Voinov, A.I. Smirnov, J. Magn. Reson. 293 (2018) 9–18.
[71] F. Mentink-Vigier, A. Collauto, A. Feintuch, I. Kaminker, V. Tarle, D. Goldfarb, J. Magn. Reson. 236 (2013) 117–125.
[72] J. Jumper, R. Evans, A. Pritzel, T. Green, M. Figurnov, O. Ronneberger, K. Tunyasuvunakool, R. Bates, A. Žídek, A. Potapenko, A. Bridgland, C. Meyer, S.A. A. Kohl, A.J. Ballard, A. Cowie, B. Romera-Paredes, S. Nikolov, R. Jain, J. Adler, T. Back, S. Petersen, D. Reiman, E. Clancy, M. Zielinski, M. Steinegger, M. Pacholska, T. Berghammer, S. Bodenstein, D. Silver, O. Vinyals, A.W. Senior, K. Kavukcuoglu, P. Kohli, D. Hassabis, Nature 596 (2021) 583–589.
[73] A.W. Senior, R. Evans, J. Jumper, J. Kirkpatrick, L. Sifre, T. Green, C. Qin, A. Žídek, A.W.R. Nelson, A. Bridgland, H. Penedones, S. Petersen, K. Simonyan, S. Crossan, P. Kohli, D.T. Jones, D. Silver, K. Kavukcuoglu, D. Hassabis, Nature 577 (2020) 706–710.
[74] M. Baek, F. DiMaio, I. Anishchenko, J. Dauparas, S. Ovchinnikov, G.R. Lee, J. Wang, Q. Cong, L.N. Kinch, R.D. Schaeffer, C. Millán, H. Park, C. Adams, C.R. Glassman, A. DeGiovanni, J.H. Pereira, A.V. Rodrigues, A.A. van Dijk, A.C. Ebrecht, D.J. Opperman, T. Sagmeister, C. Buhlheller, T. Pavkov-Keller, M.K. Rathinaswamy, U. Dalwadi, C.K. Yip, J.E. Burke, K.C. Garcia, N.V. Grishin, P.D. Adams, R.J. Read, D. Baker, Science 373 (2021) 871–876.
[75] G. Jeschke, A. Bender, H. Paulsen, H. Zimmermann, A. Godt, J. Magn. Reson. 169 (2004) 1–12.
[76] G. Jeschke, Y. Polyhach, Phys. Chem. Chem. Phys. 9 (2007) 1895–1910.
[77] J.L. Baber, J.M. Louis, G.M. Clore, Angew. Chemie Int. Ed. 54 (2015) 5336–5339.
[78] S. Milikisiyants, M.A. Voinov, A. Marek, M. Jafarabadi, J. Liu, R. Han, S. Wang, A. I. Smirnov, J. Magn. Reson. 298 (2019) 115–126.
[79] J.E. Lovett, B.W. Lovett, J. Harmer, J. Magn. Reson. 223 (2012) 98–106.
[80] S. Milikisyants, F. Scarpelli, M.G. Finiguerra, M. Ubbink, M. Huber, J. Magn. Reson. 201 (2009) 48–56.
[81] L.V. Kulik, S.A. Dzuba, I.A. Grigoryev, Y.D. Tsvetkov, Chem. Phys. Lett. 343 (2001) 315–324.
[82] D. Abdullin, M. Suchatzki, O. Schiemann, Appl. Magn. Reson. 53 (2022) 539–554.
[83] K. Keller, A. Doll, M. Qi, A. Godt, G. Jeschke, M. Yulikov, J. Magn. Reson. 272 (2016) 108–113.
[84] K. Keller, M. Qi, C. Gmeiner, I. Ritsch, A. Godt, G. Jeschke, A. Savitsky, M. Yulikov, Phys. Chem. Chem. Phys. 21 (2019) 8228–8245.
[85] T.F. Cunningham, M.R. Putterman, A. Desai, W.S. Horne, S. Saxena, Angew. Chemie Int. Ed. 54 (2015) 6330–6334.
[86] A. Giannoulis, K. Ackermann, P.E. Spindler, C. Higgins, D.B. Cordes, A.M.Z. Slawin, T.F. Prisner, B.E. Bode, Phys. Chem. Chem. Phys. 20 (2018) 11196–11205.
[87] I. Ritsch, H. Hintz, G. Jeschke, A. Godt, M. Yulikov, Phys. Chem. Chem. Phys. 21 (2019) 9810–9830.
[88] K. Ackermann, A. Giannoulis, D.B. Cordes, A.M.Z. Slawin, B.E. Bode, Chem. Commun. 51 (2015) 5257–5260.
[89] J.L. Wort, K. Ackermann, D.G. Norman, B.E. Bode, Phys. Chem. Chem. Phys. 23 (2021) 3810–3819.
[90] G. Jeschke, V. Chechik, P. Ionita, A. Godt, H. Zimmermann, J. Banham, C.R. Timmel, D. Hilger, H. Jung, Appl. Magn. Reson. 30 (2006) 473–498.
[91] K. Ackermann, A. Chapman, B.E. Bode, Molecules 26 (2021) 7534.
[92] K. Ackermann, C. Pliotas, S. Valera, J.H. Naismith, B.E. Bode, Biophys. J. 113 (2017) 1968–1978.
[93] J.L. Wort, K. Ackermann, A. Giannoulis, B.E., Bode, 2023, Enhanced sensitivity for pulse dipolar EPR spectroscopy using variable-time RIDME (dataset). Dataset. University of St Andrews Research Portal. https://doi.org/10.17630/db46fa7d-13c5-49ef-aa07-847ab67c7bca.
[94] L. Fábregas Ibáñez, G. Jeschke, Phys. Chem. Chem. Phys. 22 (2020) 1855–1868.
[95] A. Giannoulis, D.B. Cordes, A.M.Z. Slawin, B.E. Bode, Magnetochemistry 8 (2022) 43.
[96] A. Giannoulis, C.L. Motion, M. Oranges, M. Bühl, G.M. Smith, B.E. Bode, Phys. Chem. Chem. Phys. 20 (2018) 2151–2154.
[97] M. Šimėnas, J. O'Sullivan, C.W. Zollitsch, O. Kennedy, M. Seif-Eddine, I. Ritsch, M. Hülsmann, M. Qi, A. Godt, M.M. Roessler, G. Jeschke, J.J.L. Morton, J. Magn. Reson. 322 (2021).
[98] A.G. Matveeva, V.N. Syryamina, V.M. Nekrasov, M.K. Bowman, Phys. Chem. Chem. Phys. 23 (2021) 10335–10346.
[99] K. Ackermann, S. Khazaipoul, J.L. Wort, A.I.S. Sobczak, A.J. Stewart, B.E. Bode, J. Am. Chem. Soc. 145 (2023) 8064–8072.
[100] S. Brandon, A.H. Beth, E.J. Hustedt, J. Magn. Reson. 218 (2012) 93–104.
[101] S.G. Worswick, J.A. Spencer, G. Jeschke, I. Kuprov, Sci. Adv. 4 (2018) eaat5218.
[102] J. Keeley, T. Choudhury, L. Galazzo, E. Bordignon, A. Feintuch, D. Goldfarb, H. Russell, M.J. Taylor, J.E. Lovett, A. Eggeling, L. Fábregas Ibáñez, K. Keller, M. Yulikov, G. Jeschke, I. Kuprov, J. Magn. Reson. 338 (2022).
[103] L. Fábregas Ibáñez, G. Jeschke, S. Stoll, Magn. Reson. 1 (2020) 209–224.
[104] J.-B. Verstraete, J.R.J. Yong, D.L. Goodwin, W.K. Myers, M. Foroozandeh, Chem. Commun. 58 (2022) 10715–10718.
[105] G. Jeschke, Protein Sci. 27 (2018) 76–85.